REGULAR PAPER • OPEN ACCESS

Degradation of vertical GaN diodes during proton and xenon-ion irradiation

To cite this article: Hironori Okumura *et al* 2023 *Jpn. J. Appl. Phys.* **62** 064001

OPEN ACCESS
Japanese Journal of Applied Physics 62, 064001 (2023)
https://doi.org/10.35848/1347-4065/acddb4

REGULAR PAPER

Degradation of vertical GaN diodes during proton and xenon-ion irradiation

Hironori Okumura[1*], Yohei Ogawara[1], Manabu Togawa[2,3], Masaya Miyahara[2,3], Tadaaki Isobe[4], Kosuke Itabashi[2,3], Jiro Nishinaga[5], and Masataka Imura[6]

[1]Faculty of Pure and Applied Sciences, University of Tsukuba, Tsukuba, Ibaraki 305-8573 Japan
[2]High Energy Accelerator Research Organization, Tsukuba, Ibaraki 305-0801, Japan
[3]International Center for Quantum-field Measurement Systems for Studies of the Universe and Particles, Tsukuba, Ibaraki 305-0801, Japan
[4]The Nishina Center for Accelerator-Based Science, RIKEN, Wako, Saitama 351-0198 Japan
[5]Research Center for Photovoltaics, National Institute of Advanced Industrial Science and Technology, Tsukuba, Ibaraki 305-8568, Japan
[6]Research Center for Functional Materials, National Institute for Materials Science, Tsukuba, Ibaraki 305-0044, Japan

*E-mail: okumura.hironori.gm@u.tsukuba.ac.jp

Received June 2, 2022; revised April 19, 2023; accepted June 11, 2023; published online June 30, 2023

We investigated the material stability of a vertical GaN Schottky barrier diode (SBD) against proton irradiations by making real-time measurements. The reverse current gradually decreased with increasing proton fluence. The current of the GaN SBD was reduced by 18% after proton irradiations with a displacement-damage dose (D_d) of 10^{12} MeV g^{-1}. We also examined signal and current degradation occurring in a vertical GaN-on-GaN *p–n* diode (PND) during xenon-ion irradiations. The signal gradually decreased with increasing xenon-ion fluence. Xenon-ion irradiations of $D_d = 10^{12}$ MeV g^{-1} reduced the collected charge in the PND by 11%. This signal degradation was close to the current degradation in the GaN SBD caused by the proton irradiations. We found that irradiations with $D_d > \sim 10^{12}$ MeV g^{-1} degraded the performance of the GaN devices.

1. Introduction

Radiation detectors are used in high-energy physics, astrophysics, spectroscopy, security, and radiotherapy. Semiconductor radiation detectors have advantages of compactness, fast timing characteristics, and high energy resolution. In a semiconductor material, incident radiation produces electron–hole pairs. The electrons and holes diffuse to the electrodes of the detector when an electric field is applied to them, generating a signal pulse. However, some forms of radiation produce Frenkel-type defects by displacing atoms from their lattice sites, leaving vacancies, interstitials, and complexes.[1,2] Point defects form deep acceptor/donor levels, decreasing the effective donor/acceptor concentration and carrier mobilities. Prolonged exposure of semiconductor detectors to radiation reduces their charge collection efficiency (CCE), causing a loss in energy and spatial resolution. A semiconductor material with a large lattice displacement energy is preferable for the long-term stability of a detector in a high-radiation environment.

Wide-bandgap semiconductors are suitable for harsh environments because of their low intrinsic carrier density and large lattice displacement energy.[3–7] GaN is an especially attractive material for radiation detectors because of its high carrier mobility, which enhances charge carrier collection, and high atomic number, which leads to many electron–hole pairs, or a large signal. A high-sensitivity GaN radiation detector requires a vertical structure with a GaN substrate because the signal-to-noise ratio increases with increasing depletion width and decreasing leakage current. There are reports on charged particle detection using vertical GaN Schottky barrier diodes (SBDs) and *p–n* junction diodes.[8–11] The degradation of semiconductor devices by charged particles is linearly correlated to the non-ionizing energy loss (NIEL) due to the nuclear stopping component.[12] The displacement damage depends on the type, fluence, and energy of the radiation. Degradation is often determined by subjecting the device to a 1–100 MeV proton irradiation because protons effectively produce a more measurable change in device characteristics in comparison with electrons or neutrons.[13] In a vertical GaN PND, 2.5 MeV protons at a fluence of 4×10^{13} protons cm^{-2} cause the breakdown voltage to decrease by 23%,[14] and reduce the hole diffusion length by 55%.[15] Still, there are few reports on the relation between displacement damage and device characteristics for GaN.

In this study, we investigated displacement damage in GaN by irradiating a vertical SBD with protons. We also investigated signal and current degradation in vertical GaN PNDs by using xenon swift-heavy ions.

2. Prolonged exposure of GaN SBD to protons

2.1. Experimental procedure

We used a 2 inch *n*-type GaN wafer with a threading dislocation density of 5×10^6 cm^{-2}, thickness of 300 μm, and [Si] $= 2 \times 10^{18}$ cm^{-3}. A GaN SBD was directly fabricated without epitaxial growth using the GaN wafer, which was cut into a 10 mm × 10 mm piece. A 20 nm Ti/100 nm Al/10 nm Ni/50 nm Au electrode was evaporated on the backside of the sample by using electron-beam deposition, followed by thermal annealing at 800 °C for 1 min in a nitrogen ambient to form an ohmic contact. A Ni (25 nm)/Au (25 nm) electrode with a diameter of 1 mm was evaporated on the sample surface using electron-beam deposition. Current–voltage (*I–V*) characteristics were measured at RT using a parameter analyzer (Keysight B1500A) before the proton irradiations.

We built a real-time system for measuring the electrical properties, as shown in Fig. 1(a). The GaN SBD was connected to a source-measure unit (ADCMT 6247G), which was controlled remotely via a laptop. The cathode electrode was directly soldered on an Al plate. The anode electrode was bonded to a flexible board using 40 μm thick Al wire. The sample was mounted on a *XY*-axis robotic scanning system.[16] The optimized scanning speed and area were ~20 mm s^{-1} and 32 mm × 32 mm, which helped to reduce the scan non-uniformity to less than 5%. The scanning system was isolated from the environment in a temperature-controlled chamber that was maintained at −15 °C by a cold

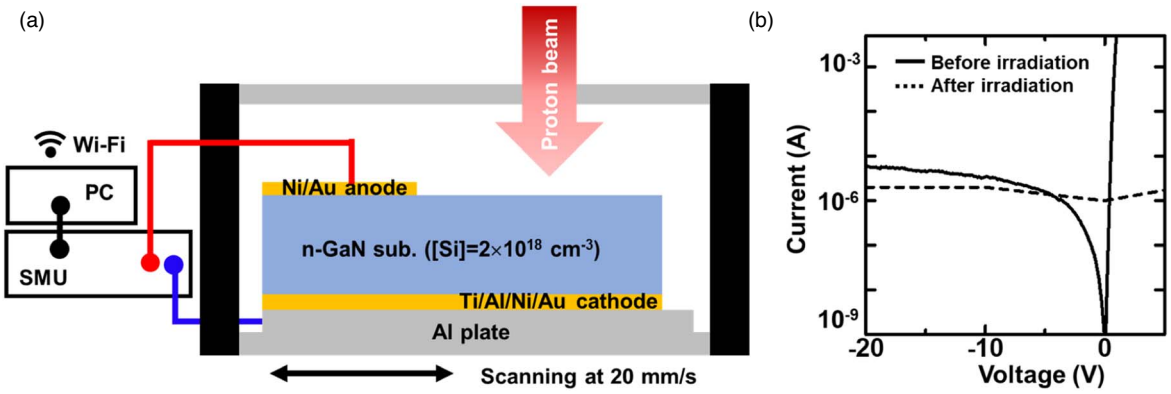

Fig. 1. (a) Real-time current measurement system of *n*-GaN SBD with 1 mm diameter Ni contact during 70 MeV proton irradiation. (b) Current–voltage characteristics of *n*-GaN SBD before and after 70 MeV proton irradiation.

nitrogen gas flow to reduce the effect of thermal agitation on the electrical characteristics.

We used a high-intensity proton beam with a momentum of 70 MeV and ∼300 nA beam current provided by the 930-type azimuthal varying field cyclotron at the cyclotron and radioisotope center facility of the Tohoku University. The scanning system enabled the proton beam, with a size of 3.5 mmϕ, to uniformly irradiate the sample plane and in depth. The delivered proton fluence (ϕ_p) was estimated from the activity of Al foils after proton irradiations using gamma rays from ^{22}Na decays. ϕ_p of 9.2×10^{15} cm^{-2} is converted to 1.4×10^{16} n_{eq} (1 MeV neutron equivalent) cm^{-2} because a 70 MeV proton induces displacement damage of 1.52 n_{eq}.[17] The stopping power (dE/dx) in GaN was calculated to be 40 MeV cm^{-1} for 70 MeV protons in a stopping and range of ions in matter (SRIM) simulation, indicating that the incident protons penetrated the GaN SBD. The equivalent total irradiation dose for the GaN SBD is estimated to be 9.6 MGy using the equation $\frac{e\phi_p}{\rho}\frac{dE}{dx}$, where e is elementary charge and ρ is density (= 6.15 g cm^{-3} for GaN).

2.2. Electrical properties of GaN SBD

The *I*–*V* characteristics of the GaN SBD before the proton irradiations are shown in Fig. 1(b). The GaN SBD showed rectifier behavior. The forward *I*–*V* characteristics were analyzed using a thermionic emission model with a Schottky barrier height of 1.0 eV and Richardson constant of 24 Acm^{-2} K^{-2}. The specific on-resistance (R_{on}) and ideality factor (n) were 6.3 Ωcm^2 and 1.5, respectively. R_{on} and n were larger than in the other reports due to the large leakage current.[18,19] The leakage current of the GaN SBD could be decreased by using a small anode electrode, a mesa structure, and a lightly donor-doped GaN epitaxial layer.

The *I*–*V* characteristics of the GaN SBD just after the proton irradiations are also shown in Fig. 1(b). The GaN SBD showed no rectifier behavior due to radiation damage. We consider that this degradation owes to radiation-induced acceptor-like defects being generated in the *n*-type region.[20] Particularly, a gallium-vacancy defect (V_{Ga}) has an acceptor level at 1.0 eV above the VB maximum and acts as a compensation center for *n*-type GaN.[21,22] Although the displacement energies of both gallium and nitrogen atoms are much less than the energy transferred to primary knock-on atoms in a high-fluence proton irradiation,[13] V_{Ga}-related defects may have primarily formed in the *n*-type GaN because of the low formation energy. Further investigation using deep-level transient spectroscopy are needed to clarify the origin of the proton-induced defects.

2.3. Degradation transition of GaN SBD

We made real-time measurements of the reverse current of the GaN SBD to investigate the material's stability to proton exposure. The current during the proton irradiations was around two orders of magnitude larger than the pre-irradiation current because electron–hole pairs were generated by the proton irradiations and thermal agitation. The measured current during the proton irradiations oscillated due to the irradiated area being shifted by the *XY*-axis scanning system. We evaluated the device degradation by using the current at concave points, at which the proton beam was the farthest from the samples. The depletion width (W_d) of a SBD is obtained by using $\boldsymbol{W_d} = \sqrt{\frac{2\varepsilon_s}{eN_D}\left(\boldsymbol{V_d} - \boldsymbol{V} - \frac{kT}{e}\right)}$, where ε_s (= $10.4\varepsilon_0$) is the dielectric constant of GaN,[23] N_D (∼[Si]) is the donor concentration, V_d (= 0.95 V) is the built-in potential,[24] V is the vias, k is the Boltzmann constant, and T is the absolute temperature. W_d of the GaN SBD is estimated to be 110 nm at $V = -20$ V.

The dependence of the current at the reverse bias of 20 V on the proton fluence (ϕ_{pe}) was estimated by assuming that the proton flux per unit time was constant. As shown in Fig. 2(a), the reverse current showed little degradation at $\phi_{pe} < 5 \times 10^{14}$ n_{eq} cm^{-2} and was close to those of the reported GaN devices.[7,13] The reverse current gradually decreased with increasing ϕ_{pe} due to the increased number of proton-induced defects. The degraded reverse current was fitted using the equation $\boldsymbol{I} = \boldsymbol{I_0}(1 + \boldsymbol{\alpha_p}\boldsymbol{\phi_{pe}})^{-\frac{1}{n}}$,[25] where I_0 is the current at the start of the irradiation, α_p is a fitting parameter defined as the damage constant, and n is another fitting parameter. According to Rose-Barnes theory, n approaches 1/3 when the current is dominated by the space charge recombination, while n approaches 2/3 when the current is dominated by diffusion.[26] The experimental data were fitted using $\alpha_p = 2.5 \times 10^{-16}$ cm^2 and $n = 0.33$, which is close to 1/3 due to the high density of recombination centers. A positive current appeared under reverse bias at a ϕ_{pe} over 6×10^{15} cm^{-2}. We consider that excess carriers that were generated by the protons and thermal agitation might have remained during the real-time *I*–*V* measurement. Hall-effect and *I*–*V* measurements should be conducted after cooling the sample in an area with less radiation to clarify the reason of the positive currents.

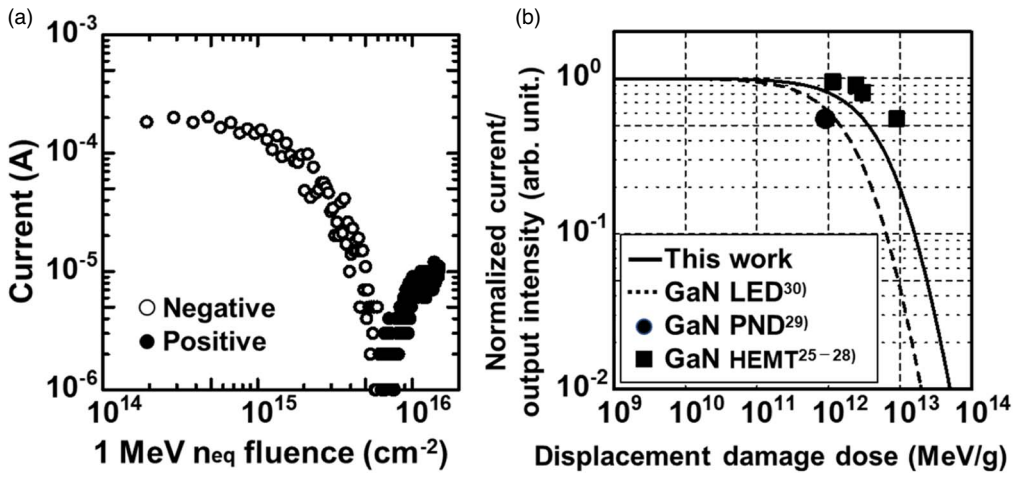

Fig. 2. (a) Reverse current of *n*-GaN SBD at reverse bias of 20 V during 70 MeV proton irradiation. (b) Relation between displacement-damage dose and normalized current of the *n*-GaN SBD fitted using Rose-Barnes theory (solid line), output intensity of GaN LED (dashed line),[30] current of GaN PND (circle),[29] and drain current of GaN HEMT (squares).[25–28]

The relation between the normalized output value of various GaN devices and the displacement damage dose (D_d), which is equal to NIEL times ϕ_p, is shown in Fig. 2(b). The plotted values include the current transition of GaN high-electron mobility transistors (HEMTs),[27–30] the current transition of the GaN PND,[31] and intensity transition of GaN LEDs.[32] The measured current during the proton irradiations should be higher than the current after the proton irradiation and cooling because the measured current includes the carriers generated by radioactivated surrounding objects and thermal agitation. However, the fitting curve was close to the reported current transitions of the GaN HEMTs and PNDs, indicating that radiation damage is dominant on the degradation transition of the GaN SBD. NIEL increases with decreasing proton energy due to the increased electronic-stopping component; SR-NIEL web calculators gave 2.3×10^{-2} MeV cm^2 g^{-1} for 2.5 MeV, 3.9×10^{-3} MeV cm^2 g^{-1} for 50 MeV, and 3.5×10^{-3} MeV cm^2 g^{-1} for 70 MeV.[33] The current of the GaN SBD fell by 18% after proton irradiations with $D_d = 10^{12}$ MeV g^{-1}. Thus, we concluded that the performance of the GaN devices was stable against proton irradiations with $D_d < \sim 10^{12}$ MeV g^{-1}. The fitting curve showed a slightly smaller degradation compared with the relation between normalized intensity and ϕ_p for a GaN LED irradiated with 50 MeV protons, for which $\alpha_p = 6.6 \times 10^{-16}$ cm^2 and $n = 0.32$ were used.[32] This smaller degradation may have resulted from the formation of complexes between the proton-induced defects and donor/acceptor dopants in the GaN LED and PND.[27–32] We need to conduct further investigations to elucidate the relation between the degradation and the structure of GaN devices.

3. Exposure of GaN PND to Xe ions

3.1. Experimental procedure

We used a GaN homoepitaxial layer grown on a 2 inch *n*-type GaN substrate with a threading dislocation density of $\sim 10^6$ cm^{-2} and [Si] $= 2 \times 10^{18}$ cm^{-3} by metal-organic CVD (SCIOCS Co., Ltd.). As schematically shown in Fig. 3(a), the PND consisted of the following layers from the top: 500 nm *p*-GaN ([Mg] $= 1 \times 10^{18}$ cm^{-3})/10 μm n^--GaN ([Si] $= 1 \times 10^{16}$ cm^{-3})/2 μm *n*-GaN ([Si] $= 1 \times 10^{18}$ cm^{-3}) layers with a 50 nm p$^+$-GaN ([Mg] $= 2 \times 10^{20}$ cm^{-3}) contact layer. After cutting the sample to the size of 5 mm $\times$ 4 mm, we fabricated the GaN PND. A 20 nm Ti/100 nm Al/10 nm Ni/50 nm Au electrode was evaporated on the backside of the sample by using electron-beam deposition, followed by thermal annealing at 800 °C for 1 min in a nitrogen ambient. After 25 nm Ni/25 nm Au electrodes were deposited, thermal annealing was carried out at 500 °C for 10 min in an oxygen ambient.[34] *I–V* and capacitance-voltage (*C–V*) characteristics were measured using a parameter analyzer. The sample was mounted on a package with silver paste. Anode electrodes were bonded to each pin with 40 μm thick Al wire.

We used a xenon beam with a momentum of 400 MeV/n provided by the heavy-ion medical accelerator in Chiba (HIMAC) located at the National Institute of Radiological Science. The GaN PND was irradiated in the air through a collimator at 1 meter from the beam duct by a ^{132}Xe beam with a size of 3–5 mmϕ. During irradiation, the xenon-ion fluence (ϕ_{xe}) was maintained to 5×10^6 particles cm^{-2} per 3.3 s pulse, which was monitored by a scintillator counter. The total xenon-ion fluence over the course of 256 min was 3×10^{10} cm^{-2}. The ion LET, given by $\frac{\frac{dE}{dx}}{\rho}$, was calculated using an SRIM simulation. From Fig. 3, the average LET in the GaN PND was estimated to be 6.3 MeV cm^2 mg^{-1}. A single-event particle effect occurs when the xenon beam strikes the GaN layers, resulting in transient signals. The charge per unit length created by an ionization is given by $\frac{dQ}{dx} = e\frac{\frac{dE}{dx}}{E_{eh}}$, where E_{eh} (=9.59 eV for GaN) is the mean electron–hole pair creation energy.[35] The charge created by a 400 MeV n^{-1} xenon ion is estimated to be 65 fC μm^{-1} for GaN. An amplifier-shaper-discriminator IC was used to read the detection signal. The number of charges detected by the GaN PND was calculated from the value of the analog-to-digital converter (ADC) peak. The detector capacitance including the coaxial cable was 22 pF. The signal was measured at RT in air by an oscilloscope (MDO4104C).

3.2. Degradation transition of GaN PND

The current density–voltage (*J–V*) characteristics of the GaN PND with an anode diameter of 1 mm are shown in Fig. 4(a).

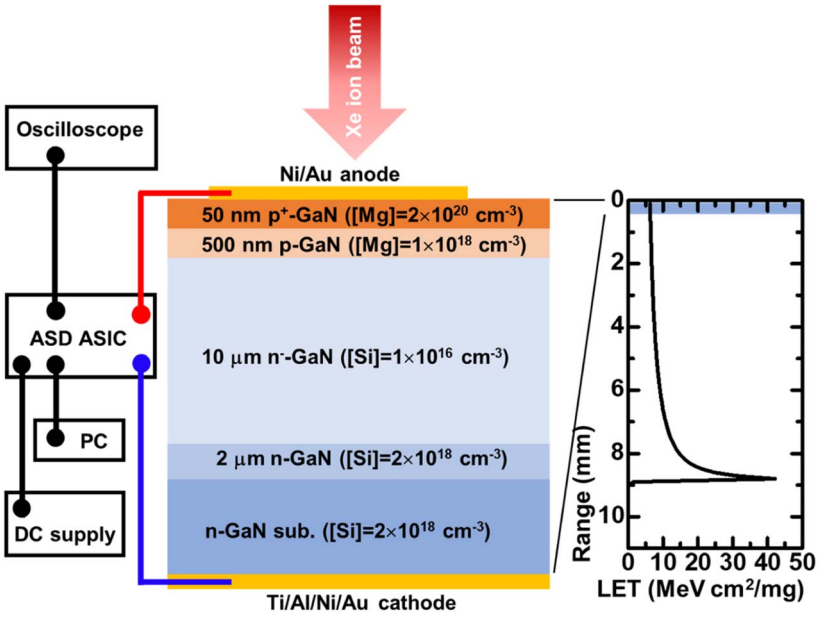

Fig. 3. Schematic cross-section of vertical GaN PND and linear energy transfer (LET) of xenon ion with 400 MeV n^{-1} in GaN at the sample depth and SRIM calculation of electronic stopping power of 52400 MeV xenon ions for GaN.

The GaN PND was fabricated without a mesa structure to minimize the effect of process damage on the electrical characteristics. The apparent turn-on voltage was 3.1 V. A forward current of 100 mA cm^{-2} was measured at 3.7 V. R_{on} was 6.8 Ωcm^2 for 100 mA cm^{-2}. The on/off current ratio was $\sim 10^3$. The large leakage current of $\sim 10^{-4}$ A cm^{-2} is attributed to the high concentration of threading dislocations, $\sim 10^6$ cm^{-2}, and the large device size having a 1 mm diameter and no mesa structure.

The ϕ_{xe} dependence of the change in displacement-damage-induced leakage current normalized to volume for the GaN PND is shown in Fig. 4(b). Here, the reverse bias was 7 V to protect the circuit from the large leakage current. Neither single-event burnout nor catastrophic failure that would have increased the leakage current were observed at this reverse bias. The increase in reverse current results from electron–hole pairs generated at damage-induced defects. The variation in leakage current is proportional to ϕ_{xe}, i.e. $\frac{\Delta I}{V_s} = \alpha_c \phi_{xe}$,[36] where V_s is the sensitive volume corresponding to the junction area times the detector thickness and α_c is a fitting parameter called the current-related damage rate. α_c was 1.7×10^{-11} A cm^{-1}, which is five orders of magnitude larger than that (10^{-17} – 10^{-16} A cm^{-1}) of a silicon detector for a 1 MeV n_{eq} flux.[36] A precise determination of α_c for a GaN detector will require a reduction in the lateral capacitance by using a guard ring.

3.3. Signal degradation of GaN PND

A single event, as shown by the ADC double peaks in Fig. 5(a), was observed at a reverse bias of 7 V. The ADC peak of 250 may be derived from the leakage current to the electrode of adjacent devices with different anode diameters. The ADC peak of 427 is evaluated to be 136 fC, which corresponds to 20% of the expectation for fully depletion of the n^--GaN layer. When the concentration of the generated carriers is smaller than the doping concentration, the total collected charges consist of carriers collected from the depletion region as drift current and carriers collected from the non-depletion region as diffusion current. In this low-injection charge collection model, the CCE is calculated from $\mathrm{CCE} = \frac{1}{E_0}\left(\int_0^{W_d} \frac{dE}{dx} dx + \int_{W_d}^{D} \frac{dE}{dx} e^{-\frac{x-W_d}{L}} dx \right)$,[37] where E_0 $(= \int_0^D \frac{dE}{dx} dx)$ is the total energy which the incident particle gives to fully depleted GaN, D ($\sim 10\,\mu$m) is the thickness of the GaN epilayer, and L (~ 250 nm) is the diffusion length of hole in n-GaN, using SRIM simulation.

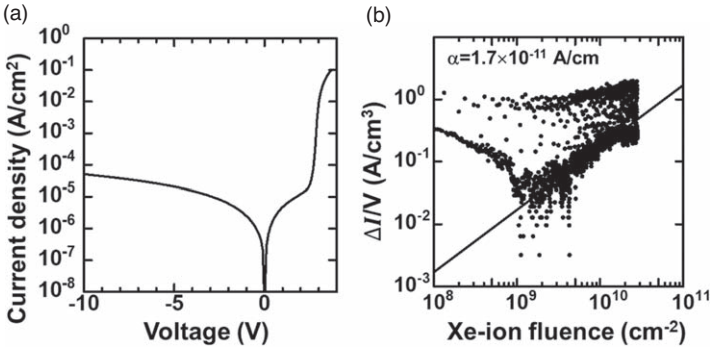

Fig. 4. (a) *J*–*V* characteristics of 1 mm diameter GaN PND. (b) Fluence dependence of leakage current for GaN PND at reverse bias of 7 V during 400 MeV n^{-1} xenon-ion irradiation.

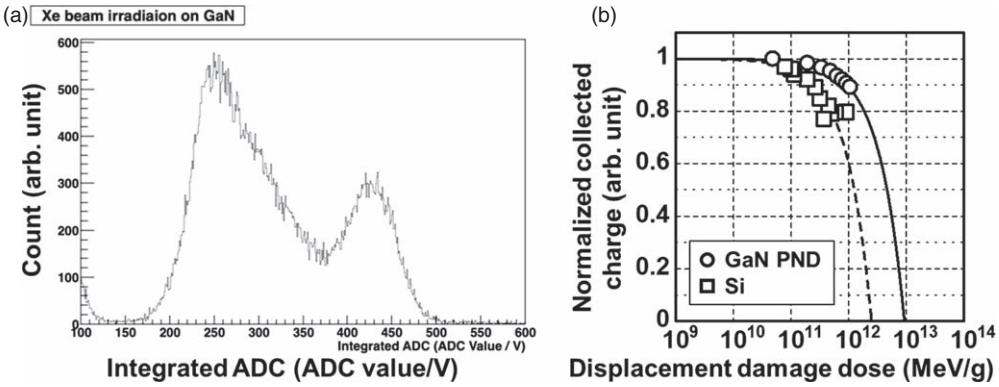

Fig. 5. (a) Outputs from 1 mm diameter GaN PND for xenon-ion irradiation. (b) Displacement-damage dose dependence of normalized corrected charges for 1 mm diameter GaN PND (circle) and Si detector (square) at reverse bias of 7 V during 400 MeV n^{-1} xenon-ion irradiation.

W_d of the GaN PND is estimated to be 729 nm at $V = -7$ V. Expected CCE of the GaN PND is calculated to be 9.8%, which is smaller than the experimental result. This discrepancy may be attributed to the carriers collected from extended drift region as drift current at a low bias.[38)]

The dependence of the normalized collected charges on D_d is shown in Fig. 5(b) for the GaN PND and Si detector. SR-NIEL web calculators indicated that NIEL increases with decreasing xenon-ion energy; 4.2×10^1 MeV cm^2 g^{-1} in GaN and 4.6×10^1 MeV cm^2 g^{-1} in Si for 400 MeV n^{-1}. After xenon-ion irradiation with a fluence of 2×10^{10} cm^{-2}, the charges collected by the Si detector and GaN PND were reduced to 80% and 92%, respectively, of their pre irradiation values. We consider that xenon-ion irradiation increases the carrier scattering and reduces the carrier lifetime due to the created trap states,[39–41)] resulting in signal degradation. The experimental data of the collected charges were fitted by $Q = Q_0(1 - \alpha_q \phi_{xe})$, where Q_0 is the charge collected at the start of the irradiation, and α_p is a fitting parameter defined as the damage constant. α_q was 1×10^{-13} cm^2 for the GaN PND and 4×10^{-13} cm^2 for the Si detector. This indicates that the GaN PND was more tolerant to the radiation than the Si detector due to the high displacement energy. The degradation of the GaN PND, despite it having channel with a high-quality epilayer, was close to that of the GaN SBD caused by the proton irradiation, indicating that the signal reduction is due to the displacement damage. We thus found that irradiations with a $D_d > \sim 10^{12}$ MeV g^{-1} dramatically degraded the performance of the GaN devices.

3.4. Signal detection using GaN PND with mesa structure

A GaN PND of the design in Fig. 3 was fabricated with a mesa termination of 600 nm depth to reduce the leakage current. The mesa termination was fabricated by reactive-ion etching at an inductively coupled plasma power of 150 W with Cl_2/BCl_3 mixing gas of 20/50 sccm under 5 Pa for 2 min after deposition of a 50 nm thick Ni mask. The J–V characteristics of the GaN PND with an anode diameter of 200 μm is shown in Fig. 6(a). The apparent turn-on voltage was 3.2 V, as expected from the bandgap energy of GaN. The GaN PND exhibited good rectifying behavior with a forward current of 100 A cm^{-2} at 3.7 V. The leakage current was dramatically reduced by the mesa isolation and small anode contact,[42)] resulting in an on/off current ratio of $\sim 10^9$. R_{on} was 5 mΩcm^2 for 100 A cm^{-2}, which is higher than the other reports, 0.1–2.3 mΩcm^2.[43–48)] R_{on} would be reduced by optimizing the fabrication process of the p-type GaN contact. The forward bias J–V characteristics were analyzed using the relation $J = J_0(e^{\frac{eV}{nkT}} - 1)$, where J_0 is the saturation current density, e is the electron charge, k is the Boltzmann constant, and T is the absolute temperature. n of the GaN PND was 2 at voltages between 2.4 and 3.2 V, because of the Shockley–Read–Hall recombination current.[49,50)] The avalanche breakdown voltage (V_B) of an ideal planar junction under the punch-through condition is calculated to be 1.5 kV from the relation $V_B = E_c W - \frac{e(N_D - N_A)W^2}{2\varepsilon_s}$, where W is the thickness of the n^--GaN drift layer, N_D–N_A the effective donor concentration, and E_c the critical electric field (=2.4 MV cm^{-1} for N_D–$N_A = 1 \times 10^{16}$ cm^{-3}).[51)] V_B measured without

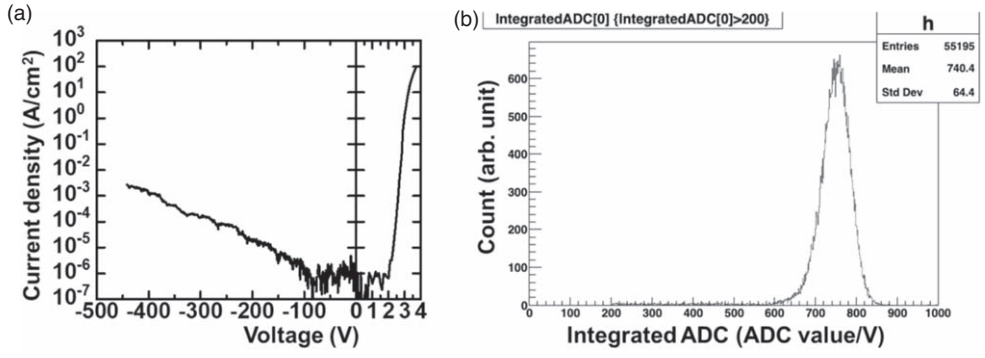

Fig. 6. (a) RT J–V characteristics of 200 μm diameter GaN PND. (b) Outputs from 200 μm diameter GaN PND for xenon-ion irradiation.

fluorinert was 444 V, which is much smaller than the calculated value. Surface passivation, good edge termination, and a field-plate structure would increase the breakdown voltage.

Signals from xenon ions were detected at a reverse bias of 50 V by using the GaN PND with the mesa structure. W_d of the GaN PND is estimated to be 1.53 μm at $V = -50$ V. Expected CCE of the GaN PND is calculated to be 17%. As shown in Fig. 6(b), a single event was observed, and a single ADC peak was obtained. The ADC peak value of 760 corresponded to 242 fC, which is 37% of what would be expected for full depletion of the n^--GaN layer. This means that the reverse bias is still small. The collected charges would be further increased by increasing a reverse bias.

4. Conclusions

We investigated the material stability of a vertical GaN SBD during 70 MeV proton irradiation by making real-time measurements of the reverse current. The current of the GaN SBD fell by 18% after the proton irradiation with $D_d = 10^{12}$ MeV g^{-1}. The reverse current gradually decreased with increasing proton fluence. We also investigated signal degradation in vertical GaN-on-GaN PND during 400 MeV n^{-1} xenon-ion irradiation. A single event was observed, showing the collected charge of 240 fC at a reverse bias of 7 V. Although the signal gradually decreased with increasing xenon-ion fluence, the degradation of the collected charges in the GaN PND was smaller than that of an Si detector. We found that the performance of the GaN devices remained stable against irradiations with displacement-damage doses $<\sim 10^{12}$ MeV g^{-1}.

Acknowledgments

This work was financially supported by the TIA "Kakehashi" collaborative research program, a project for Tsukuba industry-university collaboration promotion, and the Murata science foundation. Part of the experiments was performed under the Research Project with Heavy Ions at NIRS-HIMAC, program No. 21H455. The irradiation for assessing the radiation damage was performed at CYRIC. The authors also wish to thank the accelerator staff at HIMAC and CYRIC for supplying the excellent beams used in this work. The device fabrication was carried out at the Nano-Processing Facility at the National Institute of Advanced Industrial Science and Technology and open facility of the University of Tsukuba.

ORCID iDs

Hironori Okumura https://orcid.org/0000-0002-5464-9169
Tadaaki Isobe https://orcid.org/0000-0001-5163-030X

1) G. F. Knoll, *Radiation Detection and Measurement* (Wiley, New Jersey, 1980) 4th ed.
2) G. Lindstrom, M. Moll, and E. Fretwurst, Nucl. Instrum. Methods Phys. Res., Sect. A **426**, 1 (1999).
3) R. J. Tapper, Rep. Prog. Phys. **63**, 1273 (2000).
4) D. C. Look, Mater. Sci. Eng. **B80**, 383 (2001).
5) A. Owens and A. Peacock, Nucl. Instrum. Methods Phys. Res., Sect. A **531**, 18 (2004).
6) F. Nava, G. Bertuccio, A. Cavallini, and E. Vittone, Meas. Sci. Technol. **19**, 102001 (2008).
7) J. Wang, P. Mulligan, L. Brillson, and L. R. Cao, Appl. Phys. Rev. **2**, 031102 (2015).
8) M. Sugiura, M. Kushimoto, T. Mitsunari, K. Yamashita, Y. Honda, H. Amano, Y. Inoue, H. Mimura, T. Aoki, and T. Nakano, Jpn. J. Appl. Phys. **55**, 05FJ02 (2016).
9) Q. Xu, P. Mulligan, J. Wang, W. Chuirazzi, and L. Cao, Nucl. Instrum. Methods Phys. Res., Sect. A **849**, 11 (2017).
10) L. Zhou, Z. Lu, J. Wu, H. Jiang, L. Chen, X. Ouyang, and K. M. Lau, IEEE Electron Device Lett. **40**, 1044 (2019).
11) A. Sandupatla, S. Arulkumaran, N. G. Ing, S. Nitta, J. Kennedy, and H. Amano, Micromachines **11**, 519 (2020).
12) J. R. Srour, C. J. Marshall, and P. W. Marshall, IEEE Trans. Nucl. Sci. **50**, 653 (2003).
13) S. J. Pearton, R. Ren, E. Patrick, M. E. Law, and A. Y. Polyakov, ECS J. Solid State. Sci. Technol. **5**, Q35 (2016).
14) M. P. King et al., IEEE Trans. Nucl. Sci. **62**, 2912 (2015).
15) K. C. Collins, A. M. Armstrong, A. A. Allerman, G. Vizkelethy, S. B. Van Deusen, F. Leonard, and A. A. Talin, J. Appl. Phys. **122**, 235705 (2017).
16) K. Nakamura, Y. Arai, M. Hagihara, K. Hanagaki, K. Hara, R. Hori, M. Hirose, Y. Ikegami, O. Jinnouchi, and S. Kamada, J. Instl. **10**, C06008 (2015).
17) (https://rd50.web.cern.ch/NIEL/default.html) (accessed August 15, 2000).
18) Y. Cao, R. Chu, R. Li, M. Chen, R. Chang, and B. Hughes, Appl. Phys. Lett. **108**, 062103 (2016).
19) T. Maeda, M. Okada, M. Ueno, Y. Yamamoto, T. Kimoto, M. Horita, and J. Suda, Appl. Phys. Lett. **10**, 051002 (2017).
20) G. Lindstorm, Nucl. Instrum. Methods Phys. Res., Sect. A **512**, 30 (2003).
21) Z. Zhang, A. R. Arehart, E. Cinkllic, J. Chen, E. X. Zhang, D. M. Fleetwood, R. D. Schrimpf, B. McSkimming, J. S. Speck, and S. A. Ringel, Appl. Phys. Lett. **103**, 042102 (2013).
22) J. L. Lyons and C. G. Van de Walle, npj Comput. Mater. **3**, 1 (2017).
23) M. J. Kane, M. J. Uren, D. J. Wallis, P. J. Wright, D. E. J. Soley, A. J. Simons, and T. Martin, Semicond. Sci. Technol. **26**, 085006 (2011).
24) T. Maeda, M. Okada, M. Ueno, Y. Yamamoto, T. Kimoto, M. Horita, and J. Suda, Appl. Phys. Exp. **10**, 051002 (2017).
25) B. H. Rose and C. E. Barnes, J. Appl. Phys. **53**, 1772 (1982).
26) K. Saarinen et al., Phys. Rev. Lett. **79**, 3030 (1997).
27) A. Karmarkar, B. Jun, D. M. Fleetwood, R. D. Schrimpf, R. A. Weller, B. D. White, L. J. Brillson, and U. K. Mishra, IEEE Trans. Nucl. Sci. **51**, 3801 (2004).
28) L. Lv, J. G. Ma, Y. R. Cao, J. C. Zhang, W. Zhang, L. Li, S. R. Xu, X. H. Ma, X. T. Ren, and Y. Hao, Microelectron. Reliab. **51**, 2168 (2011).
29) B. D. Weaver, P. A. Martin, J. B. Boos, and C. D. Cress, IEEE Trans. Nucl. Sci. **59**, 3077 (2012).
30) Y. Xi et al., J. Vac. Sci. Technol. B **32**, 012201 (2014).
31) G. Vizkelethy, M. P. King, O. Aktas, I. C. Kizilyalli, and R. J. Kaplar, Nucl. Instrum. Methods Phys. Res., Sect. B **404**, 264 (2017).
32) S. M. Khanna et al., IEEE Trans. Nucl. Sci. **51**, 2729 (2004).
33) (http://Sr-niel.org/) (accessed June 15, 2023).
34) H. Okumura, D. Martin, and N. Grandjean, Appl. Phys. Lett. **109**, 252101 (2016).
35) E. B. Yakimov, A. Y. Polyakov, I. V. Shchemerov, N. B. Smirnov, A. A. Vasilev, P. S. Vergeles, E. E. Yakimov, A. V. Chernykh, F. Ren, and S. J. Pearon, Appl. Phys. Lett. **118**, 202106 (2021).
36) M. Moll, "Radiation Damage in Silicon Particle Detectors," Ph.D. Thesis Humburg University (1999).
37) M. B. H. Breese, J. Appl. Phys. **74**, 3789 (1993).
38) N. Iwamoto, S. Onoda, T. Makino, T. Oshima, K. Kojima, A. Koizumi, K. Uchida, and S. Nozaki, IEEE Trans. Nucl. Sci. **58**, 305 (2011).
39) V. V. Ursaki, I. M. Tiginyanu, O. Volciuc, V. Popa, V. A. Skuratov, and H. Morkoc, Appl. Phys. Lett. **90**, 161908 (2007).
40) L. M. Zhang, C. H. Zhang, L. Q. Zhang, X. J. Jia, T. D. Ma, Y. Song, Y. T. Yang, B. S. Li, and Y. F. Jin, Nucl. Instrum. Methods Phys. Res., Sect. B **269**, 1782 (2011).
41) P. N. M. Ngoepe, W. E. Meyer, F. D. Auret, E. Omotoso, T. T. Hlatshwayo, V. A. Skuratov, and M. Diale, Nucl. Instrum. Methods Phys. Res., Sect. B **409**, 69 (2017).
42) H. Okumura, Y. Ogawara, M. Togawa, M. Miyahara, J. Nishinaga, M. Imura, and T. Isobe, Ext. Abstr. Int. Conf. Solid State Devices and Materials, 2021, p. 199.
43) I. C. Kizilyalli, A. P. Edwards, H. Nie, D. Bour, T. Prunty, and D. Disney, IEEE Electron Device Lett. **35**, 247 (2014).
44) K. Nomoto, B. Song, Z. Hu, M. Zhu, M. Qi, N. Kaneda, T. Mishima, T. Nakamura, D. Jena, and H. G. Xing, IEEE Electron Device Lett. **37**, 161 (2016).

45) S. Usami et al., Appl. Phys. Lett. **112**, 182106 (2018).
46) J. Wang, L. Cao, J. Xie, E. Beam, R. McCarthy, C. Youtsey, and P. Fay, Appl. Phys. Lett. **113**, 023502 (2018).
47) H. Lee, Y. Zhang, Z. Chen, M. W. Rahman, H. Zhao, and S. Rajan, IEEE Trans. Electron Devices **67**, 3553 (2020).
48) H. Fu et al., IEEE Electron Device Lett. **41**, 127 (2020).
49) Z. Hu, K. Nomoto, B. Song, M. Zhu, M. Qi, M. Pen, X. Cao, V. Protasenko, D. Jena, and H. G. Xing, Appl. Phys. Lett. **107**, 243501 (2015).
50) T. Maeda, T. Narita, H. Ueda, M. Kanechika, T. Uesugi, T. Kachi, T. Kimoto, M. Horita, and J. Suda, Jpn. J. Appl. Phys. **58**, SCCB14 (2019).
51) T. Maeda, T. Narita, S. Yamada, T. Kachi, T. Kimoto, M. Horita, and J. Suda, IEEE Electron Device Lett. **43**, 96 (2021).